

# Biomagnetic detection of gastric electrical activity in normal and vagotomized rabbits

L. A. BRADSHAW,\*†,‡ A. G. MYERS,† A. REDMOND,† J. P. WIKSWO\* & W. O. RICHARDS†,§

\*Living State Physics Group, Department of Physics and Astronomy

†Department of Surgery, Vanderbilt University, Nashville, TN, USA

‡Department of Physics and Engineering, Lipscomb University, Nashville, TN, USA

§Department of Surgery, Veterans' Affairs Medical Center, Nashville, TN, USA

**Abstract** We recorded the vector magnetogram (MGG) due to gastric electrical activity (GEA) in normal rabbits using a Superconducting QUantum Interference Device (SQUID) magnetometer and measured the degree of correlation of the MGG with 24 channels of serosal electrodes. The vector magnetometer allows us to non-invasively record three orthogonal magnetic field components and project the recorded magnetic field vector into arbitrary directions. We optimized the magnetic field vector direction to obtain the highest possible correlation with each serosal electrode recording. We performed a vagotomy and examined spatial and temporal changes in the serosal potential and in the transabdominal magnetic field. We obtained spatial information by mapping the recorded signals to the electrode positions in the gastric musculature. Temporal evidence of uncoupling was observed in spectral analyses of both serosal electrode and SQUID magnetometer recordings. We conclude that non-invasive recordings of the vector magnetogram reflect underlying serosal potentials as well as pathophysiological changes following vagotomy.

**Keywords** bradygastria, electrical control activity, electrogastrogram, magnetogastrogram, slow wave, tachygastria.

## INTRODUCTION

The electrical activity of gastric smooth muscle cells consists of a rhythmic subthreshold depolarization–

repolarization known as the electrical control activity (ECA) or slow wave. In humans, the gastric slow wave oscillates with a frequency of about three cycles per minute (cpm), and is somewhat faster in rabbits, at around 5 cpm.<sup>1,2</sup> Gastric electrical activity (GEA) is propagated through regions of coupled cells from the mid-corpus towards the pylorus. Propagated wavefronts are observed in the gastric musculature with multichannel serosal or intraluminal electrodes.<sup>3,4</sup> Current research strongly implicates interstitial cells of Cajal (ICCs) as the originators of GEA with smooth muscle cells passively propagating the activity.<sup>5</sup>

Abnormal GEA has not been well studied. Although workers studying the human electrogastrogram (EGG) – the cutaneous potential associated with GEA – have reported observations of tachygastria (frequency above 4.5 cpm) and bradygastria (frequency below 2 cpm), the serosal aetiology of these observations remains under investigation.<sup>6,7</sup> Presumably, disease states can cause uncoupling of either ICCs or gastric smooth muscle cells and create independent oscillatory regions. Several authors have observed dysrhythmias in cutaneous EGG recordings. Although tachygastria is often identified in patients, bradygastria is less frequently observed, and its correlation with cutaneous EGG is not clear.<sup>8–13</sup> One condition believed to cause disruption of normal GEA is the loss of neural control by the extramural vagus nerves.<sup>14</sup>

As one may record the electric potential from smooth muscle sources, they also have a magnetic field, and these may be recorded using a Superconducting QUantum Interference Device (SQUID) magnetometer. In a previous paper, we showed that the magnetic field from intestinal smooth muscle recorded outside the abdomen correlated highly with serosal electrode recordings.<sup>15</sup> We have also shown that the changes in small bowel electrical activity caused by intestinal ischaemia are reflected in SQUID

### Address for correspondence

Alan Bradshaw, Department of Physics and Astronomy,  
Box 1807 Station B, Vanderbilt University, Nashville,  
TN 37235, TN, USA.

Tel.: +615 322 0705; fax: +615 322 4977;

e-mail: alan.bradshaw@vanderbilt.edu

Received: 21 February 2003

Accepted for publication: 5 April 2003

recordings.<sup>16</sup> We showed that SQUID recordings were able to non-invasively detect the different frequencies of gastric magnetic fields (GMFs) at about 3 cpm and intestinal magnetic fields from 8 to 12 cpm, and that the locations of these frequencies was consistent with the known slow wave frequency profile of the gastrointestinal tract.<sup>17</sup>

Additionally, the magnetic field is a vector quantity with three independent components. Measurements of the magnetic field vector from GEA allowed us to observe the direction of propagation of GEA in normal human subjects.<sup>18</sup>

Our goals for this work were threefold: (1) to determine the degree of correlation between serosal electrode and SQUID magnetometer recordings of normal GEA; (2) to investigate the potential additional information contained in the magnetic field vector components; and (3) to examine changes in GMFs associated with vagotomy.

## MATERIALS AND METHODS

### Recording setup

All animal experiments were approved by the Vanderbilt Institutional Animal Care and Use Committee. We anaesthetized eight male New Zealand white rabbits (acepromazine/xylazine/ketamine) and performed a laparotomy. A 24-channel monopolar serosal electrode platform was attached to the anterior surface of the stomach to record serosal potentials, and the laparotomy closed for baseline recordings. A reference electrode was attached to the animal's right leg. The electrode platform consisted of silver wires arranged in a  $6 \times 4$  grid with an interelectrode spacing of 1 cm to provide coverage of the entire stomach. We attached the electrodes to a bioamplifier system that bandpasses signals from 0.016 to 3 Hz. Output of the electrode amplifiers was acquired digitally (National Instruments E-6013 A/D card, Austin, Texas, USA; Dell 450 MHz Dual-Pentium III processor, Austin, Texas, USA; LabVIEW software, National Instruments, Austin, Texas, USA) with a sampling rate of 100 Hz.

Magnetic recordings were obtained from a vector SQUID magnetometer (Conductus Inc.) with two sets of three orthogonal detection coils. The two sets of detection coils provide two separate gradiometer baselines (5 and 15 cm). For our studies, we found the shorter baseline configuration provided higher signal-to-noise ratios. The SQUID magnetometer sensing system is enclosed in a vacuum dewar filled with liquid helium to make electronic components superconducting. Magnetic flux incident upon detection

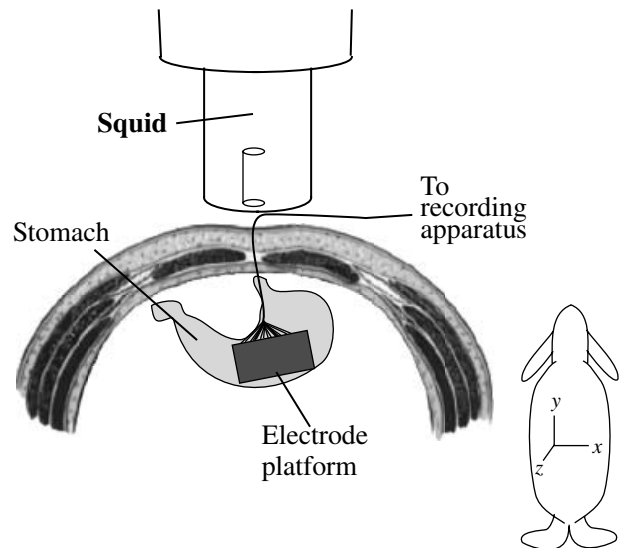


**Figure 1** Experimental set-up. We positioned the stomach in the abdomen with the 24-channel serosal electrode platform attached, and recorded serosal potentials simultaneous with  $x$ ,  $y$  and  $z$  components of the magnetic field using the Superconducting QUantum Interference Device.

coils located in the tail of the magnetometer dewar induces current in the detection coil circuit, which is again inductively coupled to the SQUID itself. The SQUID is an electronic circuit capable of producing a voltage signal that is directly proportional to the amount of incident magnetic flux. Thus, the SQUID is a magnetic flux-to-voltage converter with unrivaled sensitivity. Voltage signals from the SQUID are amplified (Conductus, IMAG), lowpass filtered at 5 Hz, and acquired digitally simultaneous with serosal electrode signals using the acquisition system described above.

We positioned the rabbits underneath the SQUID magnetometer with the detection coils located directly above the serosal electrode platform (Fig. 1). We recorded baseline signals for a minimum of 10 min, then re-opened the laparotomy incision and transected the vagal nerve. We again closed the laparotomy and replaced the animal beneath the SQUID for vagotomized recordings.

### Data analysis: correlated vector projection technique

As our signals of interest occur at frequencies below 1 Hz, we digitally filtered both electrode and magnetometer post-acquisition data from 0.016 Hz to 1 Hz. We plotted recorded serosal potentials to the mapped positions of the electrodes. One-minute samples of the signals were spectrally analysed using an autoregressive technique.

Electrical currents associated with the GEA produce vector magnetic fields. We analyse the three recorded magnetic field components by projecting them into particular directions. The direction cosines associated with a vector projection of the gastric magnetic field are defined by

$$B_{\text{proj}}(t) = \alpha \cdot \mathbf{B}(t) = \alpha_x B_x(t) + \alpha_y B_y(t) + \alpha_z B_z(t), \quad (1)$$

where the components of  $\alpha$  are the direction cosines and  $\mathbf{B} = (B_x, B_y, B_z)$  are the recorded magnetic field components. Any direction can be chosen in which to project the magnetic field, but we are most interested in the particular magnetic field projection that is associated with currents from GEA. To choose this direction, we determine the correlation between the projected magnetic field and serosal potential recordings. For each serosal electrode  $i$ ,  $i = 1, \dots, 24$ , our problem is to find  $\alpha_i$  such that

$$\int [\mathbf{B}(t) \cdot \alpha_i] V_i(t) \quad (2)$$

is maximized. Then the  $\alpha_i$  are unit vectors in the direction of the 24 vector magnetic fields whose time series optimally correspond to those in each of the 24 serosal electrodes. We expect similar waveforms from serosal potentials and external magnetic fields as the quasistatic approximation of electromagnetism holds.<sup>19</sup>

The correlated vector projections,  $\alpha_i$ , are determined using a multidimensional unconstrained nonlinear Nelder-Mead routine (MATLAB, Mathworks, Natick, MA, USA). The gastric magnetic field vector projections are then determined as

$$B_i(t) = \mathbf{B}(t) \cdot \alpha_i. \quad (3)$$

Data from these GMF vector projections may then be analysed in the same fashion as those from serosal electrode recordings.

## RESULTS

Implementation of the correlated vector projection technique is illustrated in Fig. 2, where the three components of the correlated vector projection are determined by maximizing the correlation between the projected magnetic field and the serosal potential. For the example shown, a direction vector of (0.15, 0.98 and 0.03) produced the optimally correlated GMF vector projection. In this case, the y-component of the magnetic field provided most of the correlation. This suggests that the GMF associated with the electrical activity recorded in this serosal electrode

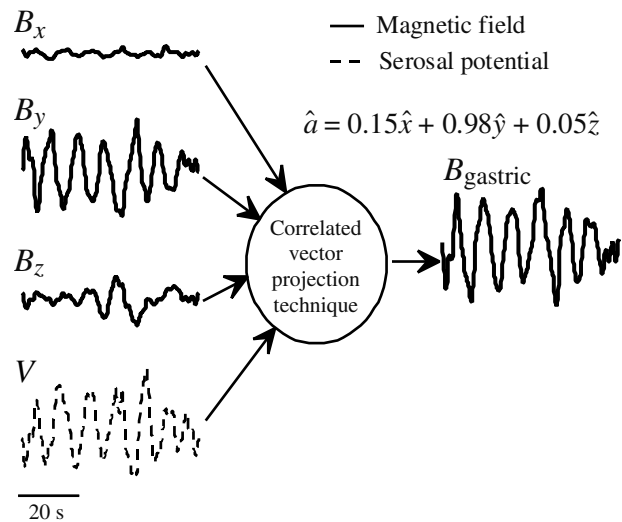


**Figure 2** Correlated vector projection technique. The  $x$ ,  $y$  and  $z$  component recordings of the magnetic field are used to project the magnetic field vector into the direction that best correlates with the recorded serosal potential. The best-fit correlation is obtained by a non-linear least-squares fit. The resulting magnetic field projection is defined as the gastric magnetic field vector projection corresponding to the serosal electrode.

was directed primarily towards the head of the animal, according to the coordinate directions shown in Fig. 1.

A typical set of baseline data from the 24 channel serosal electrode is shown in Fig. 3. The regular gastric electrical control activity with a frequency of 6.4 cpm is clearly evident in all channels. SQUID channels in the upper right are located near the oesophagus, while those in the upper left are near the duodenum. The lower right channels are along the greater curvature of the antrum, typically considered as the pacemaker region.

In the same figure, we show the waveform of the best correlated projection of the magnetic field vector at the corresponding electrode locations. The magnetic fields exhibit the same oscillatory patterns as the serosal electrodes. The numbers next to the waveforms are the correlation coefficients between the magnetic field vector and the serosal electrode recording at that location. A high degree of correlation is observed, ranging in this study from a low value of 0.216 in the lower left channel to 0.861 in the mid-corpus. Over all eight experiments, the average correlation coefficient was  $0.38 \pm 0.19$  for individual electrode channels with vector projections. However, the maximal correlation coefficient for all 24 electrodes was  $0.64 \pm 0.18$ . These data indicate that while it was not always possible to determine a GMF vector that was closely correlated

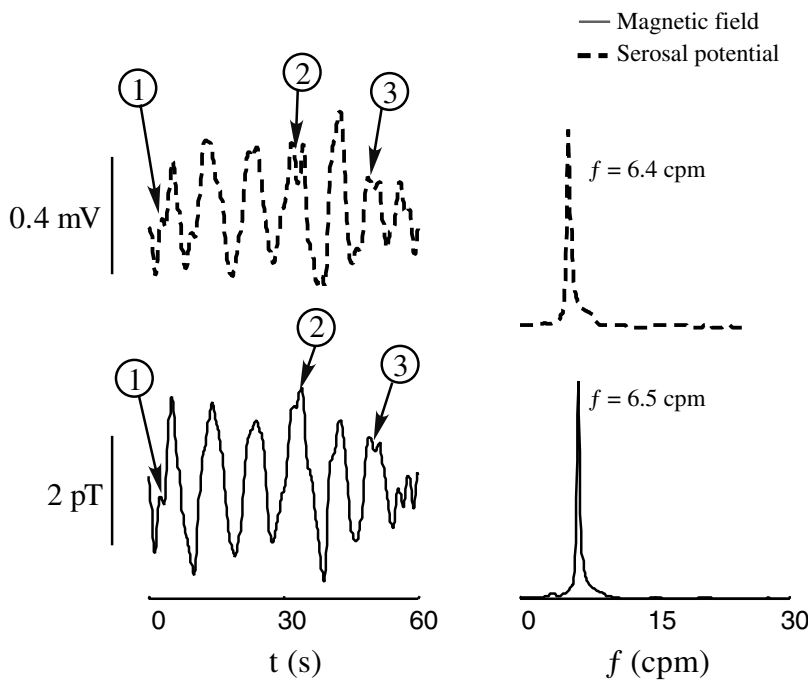


**Figure 3** Spectral analysis. Frequencies of the gastric electrical activity recorded by serosal electrodes (dashed) and the gastric slow wave vector projection from the Superconducting QUantum Interference Device (SQUID) magnetometer (solid) were determined by autoregressive spectral analysis. Note the similarity in both recorded frequency and waveform characteristics (1–3).

with each individual electrode, it was nearly always possible to determine a magnetic field vector that closely correlated with at least one electrode. These SQUID-electrode correlations were similar to the correlation between adjacent electrodes ( $0.45 \pm 0.10$ , channels 10 and 11).

The gastric slow wave frequency determined from the magnetic field vector projections closely matched those obtained by serosal electrodes. We computed the power spectra from 1-min samples of serosal potential and of the GMF vector projection (see Fig. 4). The gastric slow wave frequency was identified with peaks in the power spectra. The average gastric slow wave frequency was  $6.10 \pm 0.11$  cpm (mean  $\pm$  SEM) in serosal electrodes, while the GMF vector projection contained an average gastric slow wave frequency of  $5.97 \pm 0.11$  cpm. Fig. 5 shows a correlation coefficient of 0.74 for slow wave frequencies determined from 1-min samples taken during baseline from the serosal potential recording and from the GMF vector.

After vagotomy was performed, we observed marked changes in both electrode and SQUID recordings. Fig. 6 shows the serosal potential and GMF vectors recorded with the vagal nerve severed. There is a significant decrease in the coordination of GEA between channels post-vagotomy. We computed the correlation coefficients between two central electrodes in the array (channels 10 and 11). Before vagotomy, the average correlation coefficient was  $0.45 \pm 0.10$ . After vagotomy, the correlation dropped significantly to  $0.34 \pm 0.09$

( $P < 0.01$ ). For the corresponding magnetic field vectors, the correlations were higher, presumably because the two adjacent electrode channels tended to have similar vector projections. The prevagotomy correlation coefficient for the GMF vector projections were  $0.70 \pm 0.09$  and dropped to  $0.55 \pm 0.15$  after vagotomy ( $P < 0.001$ ).

The frequency spectrum of the serosal potential recorded in electrode 10 and the corresponding GMF vector projection are shown pre- and post-vagotomy in Fig. 7. No significant difference was noted in the dominant gastric slow wave frequency postvagotomy ( $6.10 \pm 0.11$  cpm vs  $6.09 \pm 0.18$  cpm, serosal electrodes;  $5.98 \pm 0.11$  cpm vs  $6.09 \pm 0.18$  cpm SQUID), although we did observe a postvagotomy increase in the SD of the dominant slow wave frequency (1.56 cpm pre-vagotomy to 2.30 cpm postvagotomy electrode; 1.51–2.34 cpm SQUID). Although the dominant frequency was unchanged, additional power appeared outside the normal frequency range in postvagotomy recordings. Here, there were slight differences in the results of the SQUID and serosal electrode recordings. Table 1 summarizes the results of an analysis of the percentage of signal power at bradydysrhythmic ( $<1$  SD from mean), normal (within 1 SD of mean), and tachydysrhythmic ( $>1$  SD from mean) frequencies. Both SQUID and electrode recordings have significantly less power in the normal frequency range postvagotomy. However, while the electrode recorded a significant increase in power in the bradydysrhyth-

**Figure 4** Electrode/Superconducting QUantum Interference Device (SQUID) data map. The map of serosal potentials (dashed) and associated GMF vector projections (solid) recorded in the serosal electrode platform. Twenty-three channels shown as one electrode were not in contact with the gastric tissue. Cross-correlation coefficients between SQUID and electrode data are indicated at the top right of each tracing, while channel numbers are shown at the bottom of seven-channel locations. A high correlation in the regular 6 cpm gastric activity recorded by both SQUID and electrodes is observed.

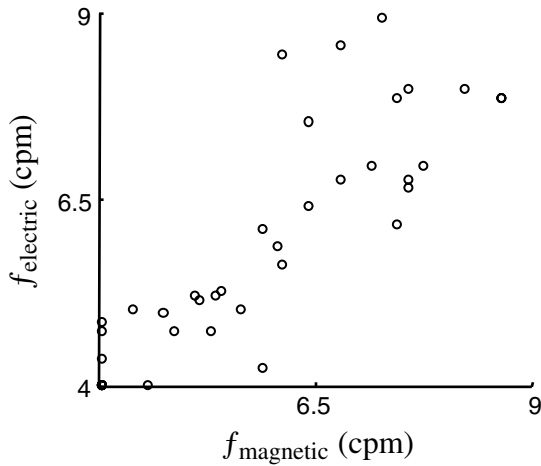
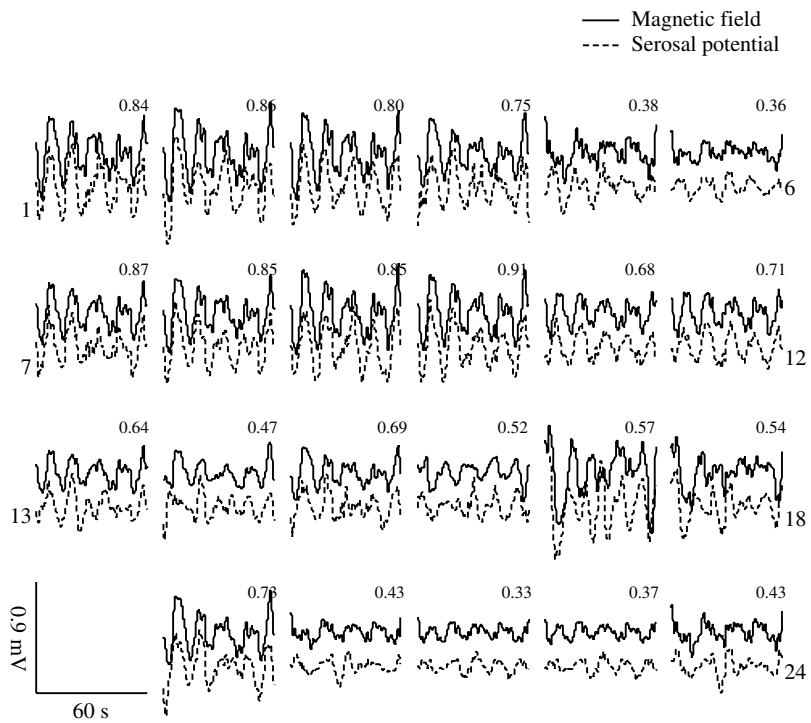


**Figure 5** Gastric electrical activity frequency correlation. Prevagotomy, the frequencies determined by the serosal electrodes were highly correlated with those determined by the Superconducting QUantum Interference Device, with a correlation coefficient of 0.74.

mic range ( $P < 0.001$ ), it did not record a significant increase in tachydysrhythmic frequencies ( $P = 0.07$ ). The SQUID magnetometer, on the contrary, recorded a significant increase in tachydysrhythmic power ( $P = 0.01$ ), but an insignificant increase in bradydysrhythmic frequencies ( $P = 0.08$ ).

The fact that multiple gastric slow wave frequencies appear postvagotomy in both SQUID and electrode power spectra suggests uncoupling of the gastric electrical syncytium. To further illustrate this, we applied a short-time Fourier-transform time-frequency analysis to electrode 10. The time-frequency representation before vagotomy (Fig. 8a) shows a consistent power in the signal centred at 6 cpm throughout the 300 s of data analysed. Post-vagotomy, the slow wave power is decreased and distributed over a wider frequency range (Fig. 8b). Peak frequencies in the power spectrum change with time, in both bradygastric and tachygastric regions. The non-stationary nature of the slow wave power distribution strongly suggests gastric electrical uncoupling.

As a final test of the ability of the vector SQUID magnetometer to recognize gastric uncoupling caused by vagotomy, we plotted the direction of the best-fit projection of the magnetic field corresponding to the serosal potential recorded in electrode 10 in Fig. 9. We found that the mean gastric magnetic field vector direction was not significantly changed after vagotomy, but the SD increased. The direction of the gastric magnetic vector may be used to infer the direction of the underlying current by the right-hand rule of magnetic fields. In this case, both pre- and post-vagotomy magnetic fields are suggestive of current propagation

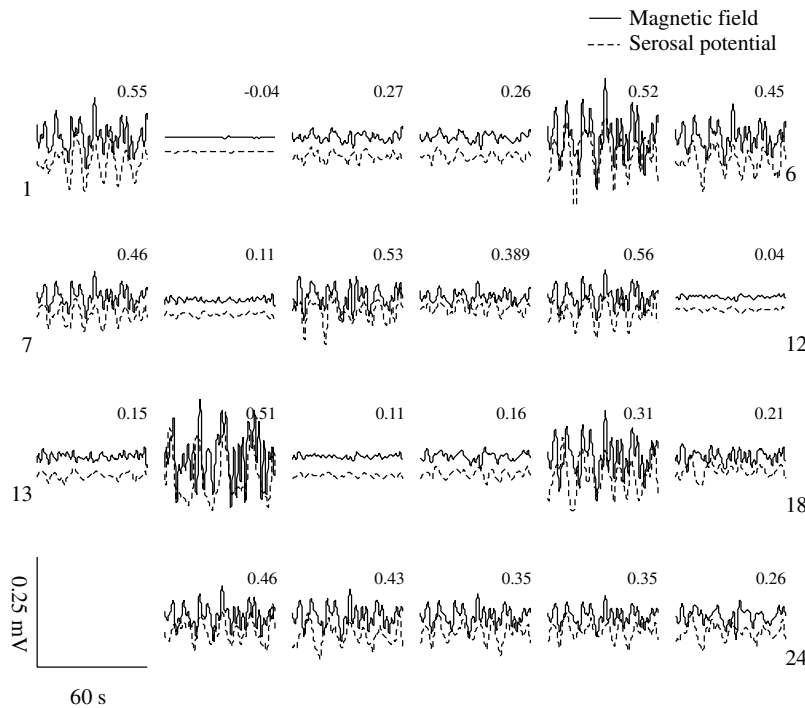


**Figure 6** Postvagotomy data maps. After vagotomy, the correlations between the serosal potentials and the best-fit gastric magnetic field (GMF) vector projections decreased. The signals recorded in the electrode array and the associated GMF projections were much less coordinated in frequency and amplitude, suggesting gastric uncoupling.

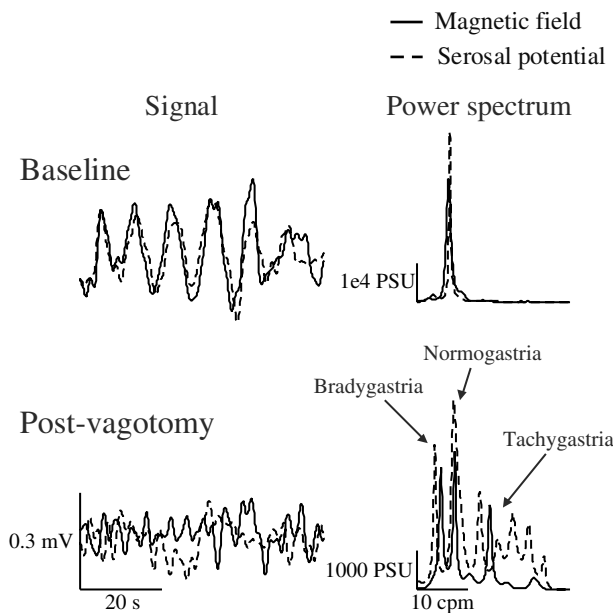


**Figure 7** Postvagotomy dysrhythmias. Gastric uncoupling caused by vagotomy leads to changes in the frequency spectrum of both serosal electrodes and the associated gastric magnetic field vectors, with frequencies appearing in the bradygastric and tachygastric region.

from right-to-left. The increase in SD suggests that the direction of the slow wave current is not as well defined after vagotomy, a condition which would result from uncoupling of the gastric syncytium.

## CONCLUSIONS

The primary conclusion is that the non-invasive magnetic recording of GEA is highly correlated with invasive serosal electrode recordings. We had previously presented similar results for intestinal electrical activity, but this is the first verification that SQUID magnetometers may also be used to record GEA. We recorded these magnetic fields using a three-sensor vector magnetometer and decomposed the orthogonal components into projections associated with GEA recorded by serosal electrodes. The results show that significant information is contained in the vector components of the gastric magnetic field, and that recordings of any single component do not correlate as highly with internal serosal potentials. Furthermore, the direction of the external gastric magnetic field vector may indicate the direction of the underlying propagation of slow wave current by the right-hand rule for magnetic fields.

The GMF vector projections suggest that vagotomy caused minor uncoupling of the gastric syncytium, which we observed most clearly in our analysis of the percentage power distribution in autoregression (AR) power spectra (Fig. 7) and in the time-frequency representations (Fig. 8). Although the mean dominant GEA frequency remained statistically unchanged, the correlation of adjacent GMF vector projections dropped significantly and a slight increase in tachydysrhythmic

**Table 1** Percentage power in Superconducting QUantum Interference Device (SQUID) projections and electrode recordings before and after vagotomy

	SQUID		Electrode	
	Prevagotomy	Postvagotomy	Prevagotomy	Postvagotomy
Bradygastric (%)	20.2	20.1	14.5	20.5
Normal (40%)	45.2	41.7	63.7	54.7
Tachygastric (%)	34.6	38.2	21.8	24.8

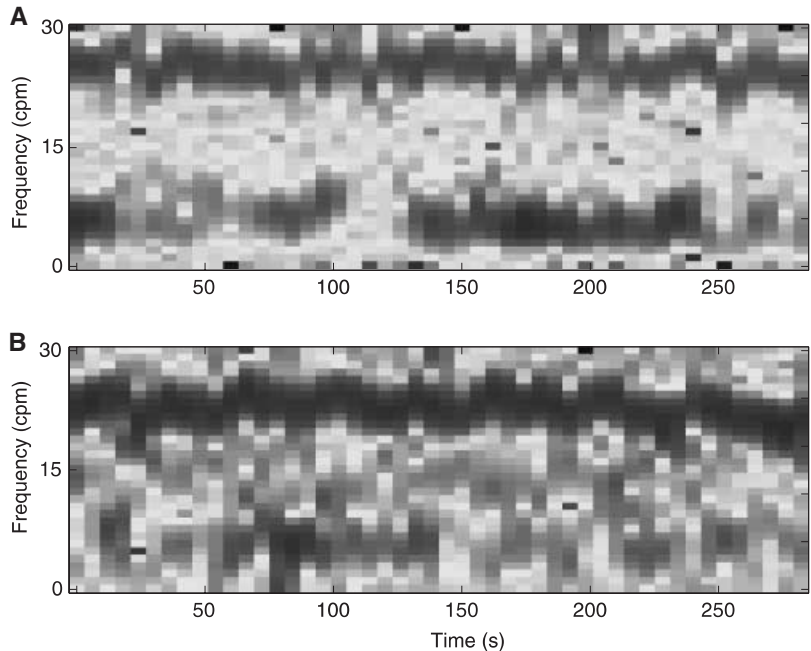


**Figure 8** Time-frequency analysis (TFA). Identification of the irregular rhythm as uncoupling is supported by TFA of a 300-s duration electrode signal (channel 10). In the stomach during baseline (A), the power in the signal is consistently near 6 cpm throughout the 300 s, while the TFA from the vagotomized stomach (B) shows that the gastric slow wave power is distributed over a wider frequency range. The dark band in the 20–30 cpm range is caused by motion associated with respiration.

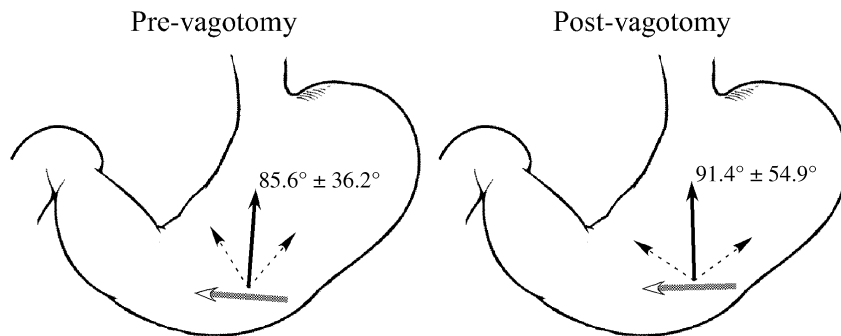


**Figure 9** Gastric slow wave magnetic field direction. The direction of the gastric slow wave vector projection associated with electrode 10 is shown for all eight animals (mean  $\pm$  SD). There is no significant difference in the baseline (A) and postvagotomy (B) mean gastric magnetic vector direction, but the postvagotomy SD in the vector direction is larger. The right-hand rule suggests that the underlying current corresponding to these magnetic vectors is directed right-to-left (grey arrows).

power was noted. These findings are consistent with earlier results from Hinder and Kelly.<sup>20</sup> We observed similar phenomena in the serosal electrode recordings. The electrodes displayed a significant postvagotomy

increase in power at bradydysrhythmic frequencies that was only borderline significant in the SQUID recordings. This was not unexpected, as the serosal potential registered a greater decrease in power at normal

frequencies than the SQUID, i.e. the invasive electrode was more specific than the SQUID in detecting uncoupling.

## DISCUSSION

These results encourage us to continue our investigation of the utility of magnetic field detection of gastrointestinal electrical activity for routine diagnosis. The SQUID magnetometer, positioned external to the subject's abdomen and without making contact, is able to record internal electrical activity in the GI musculature nearly as well as invasive serosal electrodes. We plan to direct our future efforts into determining the spatial properties of both normal and abnormal GMFs. In this study, we used a single-channel vector magnetometer recording three orthogonal magnetic field components. In future, we intend to investigate the spatiotemporal characteristics of gastrointestinal magnetic fields using a multichannel magnetometer with whole-abdomen coverage. Typically, these devices are single-component detectors that record the magnetic field component normal to the abdomen surface, but we will additionally investigate the utility of multichannel vector magnetometers in the detection of normal GEA as well as GEA during disease states involving uncoupling of the gastric smooth muscle syncytium.

## ACKNOWLEDGMENTS

This work is supported by grants from the National Institutes of Health (NIH 1 R01 DK- 58697-1) and the Department of Veterans' Affairs Research Service.

## REFERENCES

- 1 Smout AJPM, van der Schee EJ, Grashuis JL. What is measured in electrogastrography? *Dig. Dis Sci* 1980; **25**: 179–87.
- 2 Christensen J, Rick GA, Lowe LS. Distributions of interstitial cells of Cajal in stomach and colon of cat, dog, ferret, opossum, rat, guinea pig and rabbit. *J Auton Nerv Syst* 1992; **37**: 47–56.
- 3 Kelly KA, Code CF, Elveback LR. Patterns of canine gastric electric activity. *Am J Physiol* 1969; **217**: 47–56.
- 4 FAMILONI BO, KINGMA YJ, BOWES KL. Study of transcutaneous and intraluminal measurement of gastric electrical activity in humans. *Med Biol Eng Comput* 1987; **25**: 397–402.
- 5 Ordog T, Baldo M, Danko R, Sanders KM. Plasticity of electrical pacemaking by interstitial cells of Cajal and gastric dysrhythmias in W/W mutant mice. *Gastroenterology* 2002; **123**: 2028–40.
- 6 Kim TW, Beckett EA, Hanna R *et al.* Regulation of pacemaker frequency in the murine gastric antrum. *J Physiol* 2002; **538**(Pt. 1): 145–57.
- 7 Mintchev MP, Bowes KL. Do increase electrogastrographic frequencies always correspond to internal tachygastria? *Ann Biomed Eng* 1997; **25**: 1052–8.
- 8 Code CF, Marlett JA. Modern medical physiology: canine tachygastria. *Mayo Clin Proc* 1974; **49**: 325–32.
- 9 Telander RL, Morgan KG, Kreulen DL. Human gastric atony with tachygastria and gastric retention. *Gastroenterology* 1978; **75**: 495–501.
- 10 You CH, Chey WY, Lee KY. Gastric and small intestinal myoelectrical dysrhythmia associated with chronic intractable nausea and vomiting. *Ann Intern Med* 1981; **95**: 449–51.
- 11 Chen J, Richards R, McCallum RW. Frequency components of the electrogastrogram and their correlations with gastrointestinal motility. *Med Biol Eng Comput* 1993; **31**: 60–7.
- 12 van der Schee ET, Grashuis JL. Contraction-related, low-frequency components in canine electrogastrographic signals. *Am J Physiol* 1986; **250**: 470–5.
- 13 Abell TL, Malagelada J-R. Glucagon-evoked gastric dysrhythmias in humans shown by an improved electrogastrographic technique. *Gastroenterology* 1985; **88**: 1932–40.
- 14 Papisova M, Atanassova E. Electrical activity of the stomach: nervous control. *Scand J Gastroenterol Suppl* 1984; **96**: 45–53.
- 15 Bradshaw LA, Allos SH, Wikswo JP Jr, Richards, WO. Correlation and comparison of magnetic and electric detection of small intestinal electrical activity. *Am J Physiol* 1997; **35**: 1159–67.
- 16 Richards WO, Garrard CL, Allos SH, Bradshaw LA, Staton DJ, Wikswo JP Jr Noninvasive diagnosis of mesenteric ischemia using a SQUID magnetometer. *Ann Surg* 1995; **221**: 696–705.
- 17 Richards WO, Bradshaw LA, Staton DJ *et al.* Magnetoenterography (MENG): noninvasive measurement of bioelectric activity in human small intestine. *Dig Dis Sci* 1996; **41**: 2293–301.
- 18 Bradshaw LA, Staton DJ, Ladipo JK, Richards WO, Wikswo JP Jr. The human vector magnetogastrogram and magnetoenterogram. *IEEE Trans Biomed Eng* 1999; **46**: 959–70.
- 19 Plonsey RW. *Bioelectric Phenomena*. New York: McGraw-Hill, 1969.
- 20 Hinder RA, Kelly KA. Human gastric pacesetter potential. Site of origin, spread, and response to gastric transection and proximal gastric vagotomy. *Am J Surg* 1977; **133**: 29–33.